Available online at www.sciencedirect.com
ScienceDirect
Ceramics International 37 (2011) 1889–1894
CERAMICS INTERNATIONAL
www.elsevier.com/locate/ceramint

Nanocrystalline In_2O_3–SnO_2 thick films for low-temperature hydrogen sulfide detection

Huan Liu, Shuxi Wu, Shuping Gong, Jun Zhao, Jianqiao Liu, Dongxiang Zhou *

Engineering Research Center for Functional Ceramics of the Ministry of Education, Department of Electronic Science & Technology, Huazhong University of Science & Technology, No. 1037 Luoyu Road, Hongshan District, Wuhan City 430074, PR China

Received 11 January 2011; received in revised form 9 February 2011; accepted 11 February 2011
Available online 19 February 2011

Abstract

Nanocrystalline In_2O_3–SnO_2 thick films were fabricated using the screen-printing technique and their responses toward low concentrations of H_2S in air (2–150 ppm) were tested at 28–150 °C. The amount of In_2O_3-loading was varied from 0 to 9 wt.% of SnO_2 and superb sensing performance was observed for the sensor loaded with 7 wt.% In_2O_3, which might be attributed to the decreased crystallite size as well as porous microstructure caused by the addition of In_2O_3 to SnO_2 without structural modification. The interfacial barriers between In_2O_3 and SnO_2 might be another major factor. Typically, the response of 7 wt.% In_2O_3-loaded SnO_2 sensor toward 100 ppm of H_2S was 1481 at room temperature and 1921 at optimal operating temperature (40 °C) respectively, and showed fast and recoverable response with good reproducibility when operated at 70 °C, which are highly attractive for the practical application in low-temperature H_2S detection.

Keywords: SnO_2; Nanocrystalline; Thick film; H_2S

1. Introduction

Wide-bandgap semiconducting oxides typified by SnO_2, ZnO, TiO_2, In_2O_3 etc. have attracted enormous research interests due to their high activity, low cost, non-toxicity, as well as ideal chemical stability [1,2]. The particularly noteworthy point is that their properties could be well tailored by introducing nanostructures or foreign materials, offering flexible application potentials in chemical sensors, physical transducers, optoelectronic and magnetoelectronic devices [3–5]. In the field of gas sensors, semiconducting oxides have been frequently used to detect combustible (e.g., H_2, CH_4) and toxic gases (e.g., CO, H_2S) from a change in the electrical resistance. SnO_2-based gas sensors, while having lower operating temperatures than other oxides, are usually operated at about 350–400 °C so as to ensure suitable sensitivity and recoverability of the response. Actually the response speed of these sensors, especially at low gas concentrations, is rather low. A more serious problem is the long recovery time and poor long-term reproducibility at low temperatures [6,7].

Therefore, many studies have been devoted to low-temperature gas detection through electronic and chemical modification of SnO_2 ceramics [8,9]. In the case of H_2S, a hazardous gas even at sub-ppm or ppb levels, the pioneering studies by Yamazoe et al. has shown that CuO is a unique excellent promoter as compared to other additives such as SrO, NiO, CaO and ZnO, which might be ascribed to the p–n heterojunction sensing mechanism [10,11]. Patil and Patil found that CuO-modified (0.6885 mass%) SnO_2 sensor showed the response of 10^5 to 300 ppm of H_2S gas at room temperature but it was essential to heat it in atmosphere up to 250 °C to recover its initial status [12]. In our previous study, the 3 at.% Cu-loaded nanocrystalline SnO_2 thin films fabricated by sol–gel dip coating technique were highly sensitive to H_2S gas at room temperature and the recoverability of the thin films appeared when the temperature raised to 50 °C [13].

Recently, In_2O_3–SnO_2 nanocomposite emerges as a novel gas-sensing material toward nitrogen oxide [14–16], carbon monoxide [17,18], ethanol [19,20], hydrogen [21,22], methane [23], and formaldehyde [24]. The potential for tunable sensitivity and selectivity of In_2O_3–SnO_2 nanocomposite

* Corresponding author.
E-mail address: huan@mail.hust.edu.cn (D. Zhou).

0272-8842/$36.00
doi:10.1016/j.ceramint.2011.02.005

toward different gases encourages us to explore the possibility to develop novel H_2S gas sensors which has not been so far reported. In this context, we demonstrated that superb sensing performance toward low concentrations of H_2S at relatively low temperatures could be achieved by the addition of In_2O_3 to SnO_2 nanocrystals as a secondary component. The sensing mechanism was discussed to understand the effect of In_2O_3 loading.

2. Experimental

2.1. Sample preparation

Laboratory-synthesized SnO_2 and In_2O_3 nanopowders via hydrothermal process were used for the preparation of sensor samples. SnO_2 nanopowder was prepared from metallic Sn, nitric acid and ammonia solution via the process reported earlier and the average crystallite size was about 3.7 nm [25]. Similarly, 0.3 g of commercial In_2O_3 powder (99.99%) was mixed with 50 mL of nitric acid solution (65 wt.% in H_2O) and 150 mL of deionized water. Ammonia solution was slowly added until the pH value of the mixture was maintained between 7 and 8. The mixture was then transferred to a Teflon-lined stainless steel autoclave and hydrothermally treated at 160 °C for 10 h. The resultant precipitates were centrifugally washed with ethanol and deionized water, and then dried at 80 °C in air for 3 h. Subsequent calcination at 300 °C in air for 2 h and slight pulverization resulted in In_2O_3 nanopowder.

The thick-film sensor samples were fabricated using standard screen-printing technology. Various amount (0, 1, 3, 5, 7 and 9 wt.%) of In_2O_3 was mixed with SnO_2 nanopowder using a terpineol-based solvent consisting of ethyl cellulose and dibutyl phthalate to form a printable viscous paste. The paste was screen-printed on planar 96%-alumina ceramics substrates previously provided with interdigited Ag–Pd electrode, dried at 120 °C for 0.5 h and sintered at 700 °C in air for 2 h.

2.2. Characterization

X-ray diffraction (XRD) analysis was performed on nanopowders as well as thick films using a diffractometer (X'Pert pro, PANalytical B V, Holland) with CuKα radiation in the 2θ range of 20°–80°. The average crystallite size (D) was calculated from XRD peaks based on the Scherrer equation as follows: $D = 0.9\lambda/B\cos\theta$, where λ, B and θ are the X-ray wavelength of the radiation used (CuKα, λ = 1.5418 Å), the full width at half maximum (FWHM) of the diffraction peak, and the Bragg diffraction angle, respectively. The microstructure of the thick films was observed using scanning electron microscope (SEM) (Sirion 200, FEI, Holland).

The response of thick-film sensors toward H_2S gas in air (2–150 ppm) was tested at 28–150 °C using a static system (QMCS-I, HUST, China) [13] where the gas concentration was determined by the volume ratio. The sensor sample was mounted over the test board and connected in series with a signal resistor so that the sensor response could be measured by continuously recording the output voltage (V_o) of the signal resistor. The response (S) of the sensors is defined as the ratio of the steady value of the sensor resistance in the air to that in the target gas. In addition to the H_2S gas, 1000 ppm of CO and 1000 ppm of CH_4 were also used to evaluate the response selectivity.

3. Results

3.1. Structural and microstructure analysis

Fig. 1 shows the XRD patterns of hydrothermally synthesized SnO_2 and In_2O_3 nanopowders indexed with tetragonal rutile structured SnO_2 (JCPDS Card No. 21-1250) and cubic structured In_2O_3 (JCPDS Card No. 71-2194) respectively. To fabricate nanocrystalline thick-film gas sensor, it is important to maintain the small crystallite size during the film sintering process. Accordingly, the XRD patterns of thick films with different loading amount of In_2O_3 are shown in Fig. 2. It can be seen that most XRD peaks of all the film samples with In_2O_3 loading belonged to SnO_2 and the substrate material Al_2O_3, along with two peak of In_2O_3. An increase in the intensity of In_2O_3 peak with increasing loading amount was observed but there were no new phases of indium and tin for all the samples, suggesting that within the loading amount investigated in this study, indium might not be incorporated into the SnO_2 lattice, which could be associated with the small amount of substitutional and interstitial solubility of In_2O_3 in SnO_2. As the ionic radius of In^{3+} (0.80 Å) is considerably different from that of Sn^{4+} (0.69 Å), substitutional dissolution of In^{3+} into the SnO_2 lattice is difficult. The interstitial mechanism of indium incorporation is not favored either considering the fact that interstitial sites in SnO_2 unit cell are certainly smaller that the ionic sites [26].

The average crystallite size of SnO_2 estimated from XRD patterns was calculated to be 8.1, 7.3, 6.1, 5.4, 4.9 and 6.0 nm respectively for of thick-film samples with increasing In_2O_3-

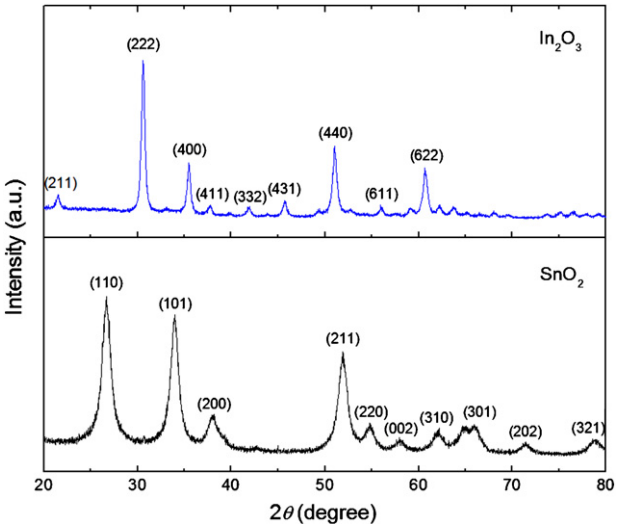

Fig. 1. XRD patterns of hydrothermally synthesized SnO_2 and In_2O_3 nanopowders.

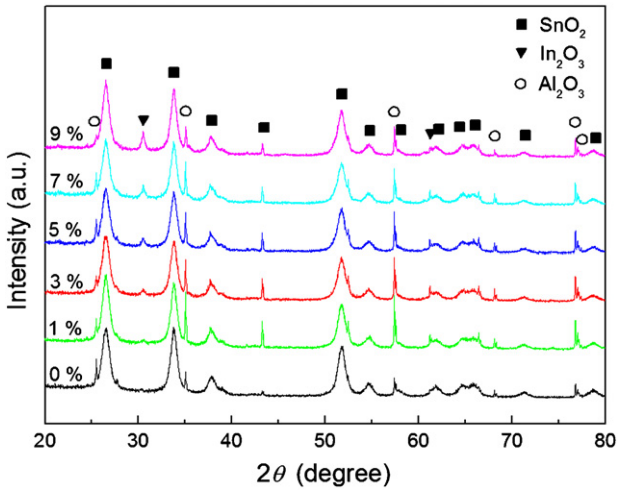

Fig. 2. XRD patterns of thick films with different amount of In_2O_3 loading by weight.

loading from 0 to 9 wt.%. We noticed that the crystallite size of pure SnO_2 increased from 3.7 nm to 8.1 nm after the sintering process for the film formation. However, the crystallite size decreased with increasing In_2O_3 loading up to 7 wt.%. This indicated that an appropriate amount of In_2O_3 loading had a distinct role in suppressing the crystallite growth of SnO_2 without structural modification, which would be highly desirable for enhanced gas-sensing performance. It is not clear why excessive loading amount like 9 wt.% resulted in larger crystallite size. A possible explanation may be that at higher content, In_2O_3 nanocrystals are more liable to aggregate, resulting in a poor dispersion on SnO_2 surfaces which weakens the role of In_2O_3 as the crystallite growth inhibitor.

Fig. 3 shows the SEM images of pure and In_2O_3-loaded SnO_2 thick films. The film morphology based on pure hydrothermal-synthesized SnO_2 nanopowder was slightly different from that in our previous study [27] as no glass frit was added to the films in this study. Here, while both constituted by sphere-like particles (aggregates) due to the agglomeration of oxide nanocrystals, the 7 wt.% In_2O_3-loaded SnO_2 thick films had smaller aggregates as compared to the pure samples. This demonstrated the ability of In_2O_3-loading to inhibit the agglomeration of SnO_2 nanocrystals.

Based on the XRD and SEM analysis, we proposed that In_2O_3 might exist as fine particles dispersed on the surface of SnO_2 nanocrystals, which acts as an obstacle for the diffusions of SnO_2 nanocrystals through the surface and grain-boundaries, and thus hindering the mass transport mechanism of sintering. As a result, the crystallite growth and agglomeration of SnO_2 nanocrystals during the sintering process were suppressed.

3.2. Response behaviors

Fig. 4 shows the response of the thick-film sensor toward 30 ppm of H_2S gas as a function of the loading amount. To show clearly the effect of In_2O_3-loading amount, the crystallite size of the samples was also plotted. As the loading amount increased to 7 wt.%, the sensor response monotonically increased and reached maximum value at 7 wt.% where the crystallite size of SnO_2 was the smallest. Further decrease in response of the 9 wt.% In_2O_3-loaded SnO_2 sensor might be associated with its larger crystallite size.

The response of 7 wt.% In_2O_3-loaded SnO_2 sensor upon H_2S gas exposure at different temperatures from room temperature (28 °C) to 150 °C was tested in order to figure out the optimal operating temperature. Corresponding values of sensor response toward 100 ppm of H_2S at these temperatures was calculated and plotted in Fig. 5. Noteworthily, the 7 wt.% In_2O_3-loaded SnO_2 sensor was highly sensitive even at room temperature, with the response of 1481 toward 100 ppm of H_2S. The 7 wt.% In_2O_3-loaded SnO_2 sensor showed maximum response of 1921 to 100 ppm of H_2S at 40 °C. At higher temperatures, the increasing rate of desorption might account for the decrease in response as the 'effective' amount of gas that could react with sensing materials tend to decrease. The optimal operating temperature around 40 °C was rather low as compared to pure SnO_2 (around 150 °C) [27], suggesting that the In_2O_3-laoding favors the adsorption of H_2S gas at lower temperatures.

For the practical application in gas detection, the selectivity and the response-recovery characteristic of gas sensors are extremely important. We examined the transient response of the sensor upon sequential exposure to 1000 ppm of CH_4, 1000 ppm of CO and 2 ppm of H_2S (Fig. 6). No obvious response to 1000 ppm of methane and carbon monoxide was

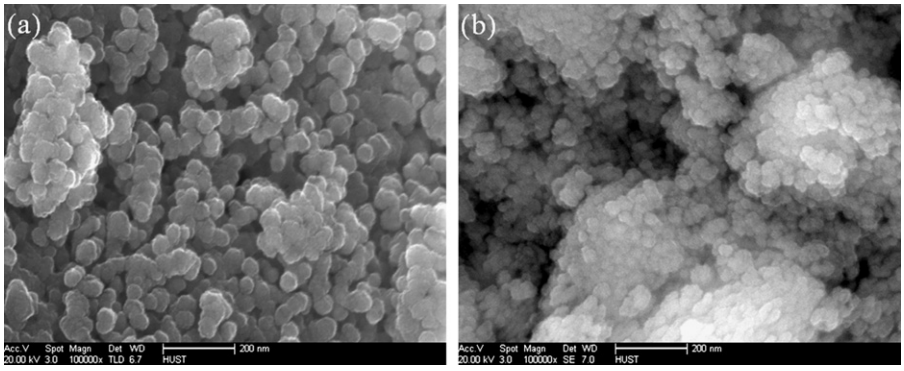

Fig. 3. SEM images of (a) pure and (b) 7 wt.% In_2O_3-loaded SnO_2 thick films.

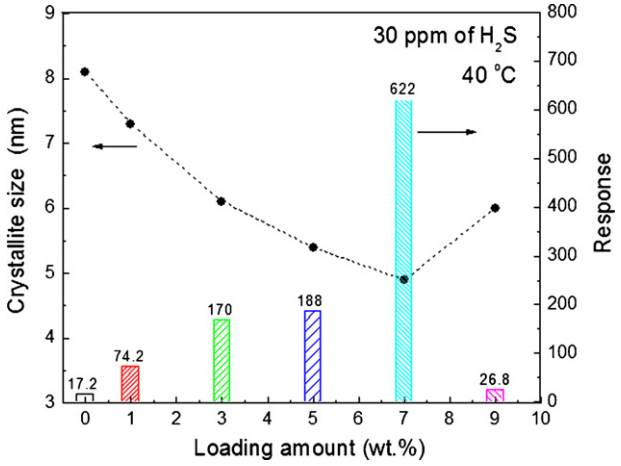

Fig. 4. Dependence of the crystallite size and sensor response on In_2O_3-loading amount.

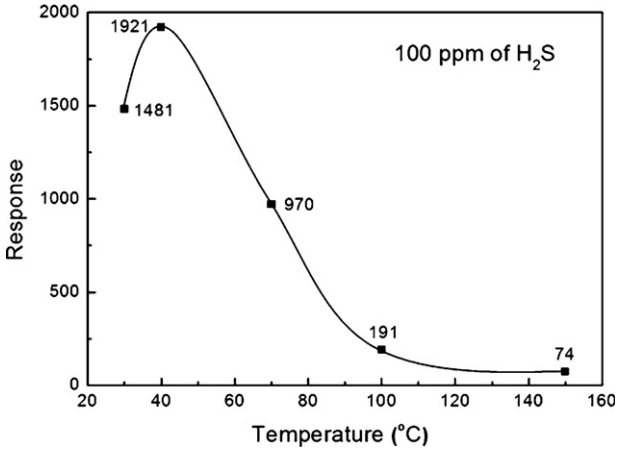

Fig. 5. Sensor response at different operating temperatures.

observed, indicating good response selectivity toward low concentrations of H_2S gas in air. We also observed that while it was difficult for the 7 wt.% In_2O_3-loaded SnO_2 sensor to recover to its initial value when operated at 40 °C, a decent recovery behavior appeared when the sensor was heated to 70 °C. The response and recovery curve toward H_2S at 70 °C is shown in Fig. 7. It can be seen that the reproducibility of the response for several gas 'In–Out' cycles was achieved due to the good recoverability, which is highly promising for the low-temperature H_2S gas detection. Therefore, the superb response behaviors of nanocrystalline 7 wt.% In_2O_3-loaded SnO_2 thick-film sensor toward low concentrations of H_2S gas have been demonstrated.

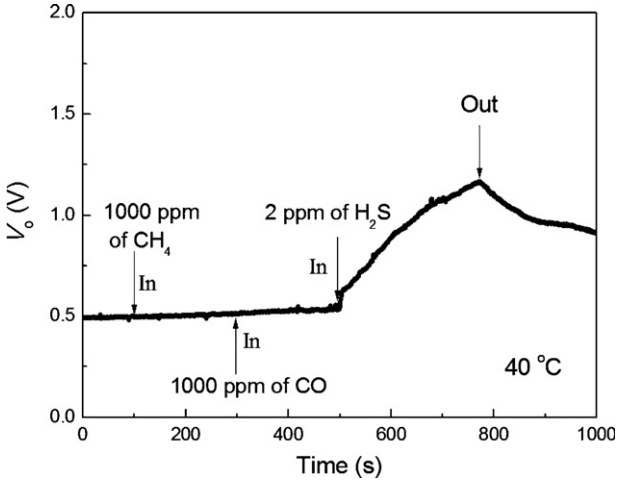

Fig. 6. Transient response curve of 7 wt.% In_2O_3-loaded SnO_2 sensors toward different gases.

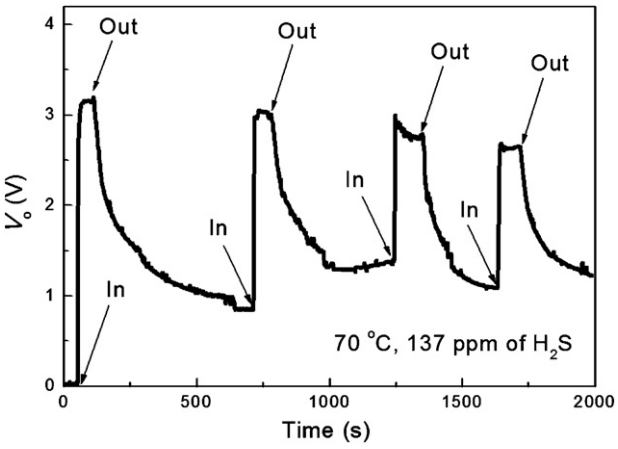

Fig. 7. Response and recovery curve of 7 wt.% In_2O_3-loaded SnO_2 sensors toward H_2S at 70 °C.

4. Discussion

According to the generally accepted model [28], the chemisorption of oxygen creates surface acceptor states and hence induces the space charge layer on oxide surfaces, leading to double potential barriers on grain boundaries where electrons are depleted. On contact with inflammable or reducing gases like H_2S, the chemisorbed oxygen would be consumed due to the reaction with the gas and as a result, the height of the potential barriers on grain boundaries decreases, releasing electrons to oxides and the electrical resistance of the sensor decreases. It should be noted that the above model focuses on the way how oxide crystallites (grains) or grain boundaries respond to a target gas, where each crystallite or grain boundary has been assumed as if it were located in an open space [29]. However, this is not the real case for thick-film gas sensors where a large number of oxide crystallites tends to aggregate and the target gas adsorbed on the surface has to diffuse through the sensing body. The nanocrystals located deep inside the aggregates may remain totally intact or inaccessible for the target gas, H_2S in this study, resulting in a loss in active surface areas and degrading the response behaviors. Therefore, a porous microstructure is much desirable since it would facilitate the process of gas adsorption, and diffusion. This might explain the superior sensing performance of 7 wt.% In_2O_3-loaded SnO_2 as compared to the pure samples which have larger aggregates as stated in the SEM analysis.

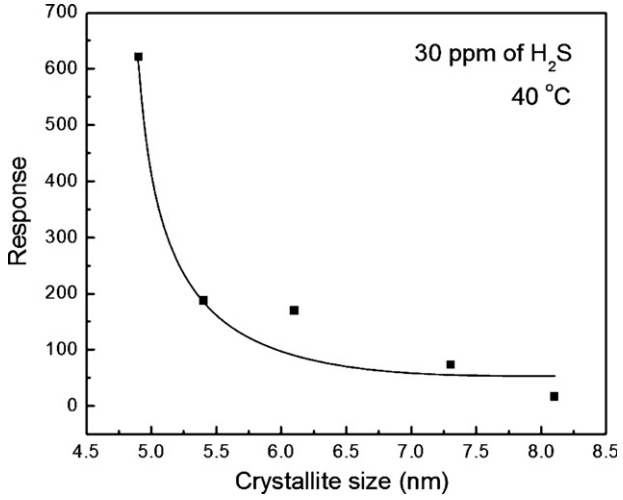

Fig. 8. Sensor response as correlated with the crystallite size.

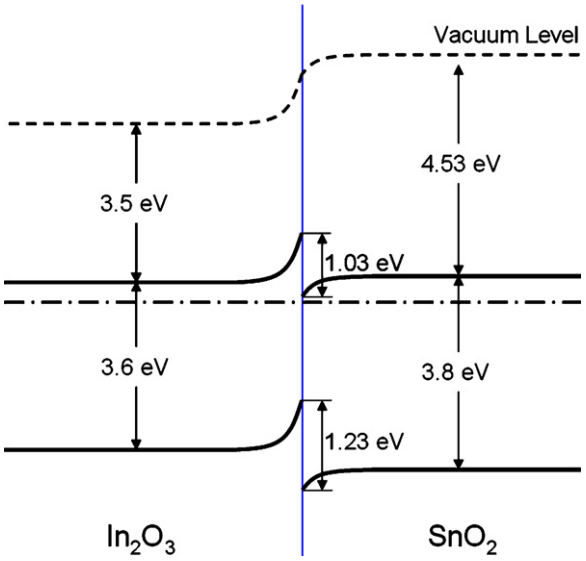

Fig. 9. An example of possible band diagram of In_2O_3–SnO_2 interfaces.

It has been indicated that the sensor response reached maximum value at 7 wt.% of In_2O_3 loading, accompanied by the smallest crystallite size among all the samples. To further reveal grain size effect, we correlated the sensor response with the crystallite size in Fig. 8. From the result of non-linear fitting, it can be seen that a decrease in crystallites size caused gradual increase of response and a further decrease to ~6 nm resulted in sharp increase of response, which was considered to be associated with the formation of an electron-depleted space charge layer that penetrates into the crystallite completely. Based on existing theory, the critical crystallite size inducing a sharp increase of response corresponds to a value equal to twice the space charge layer thickness [30,31]. Here, for the crystallite size below 6 nm, the whole regions of each SnO_2 crystallite might become depleted with the electrons. As a result, the overall electrical resistance of the gas sensor increased abruptly and was mainly controlled by the bulk resistance of each crystallite which strongly depended on the crystallite size. Therefore, the sensor response would increase drastically with the crystallite size below the critical value. Our experimental results predicts that controlling the crystallite size below 6 nm might be a great opportunity for designing and developing high-performance gas sensors. Although this is not always practical because nanocrystals tend to grow at elevated operating temperatures which might induce serious degradation in sensor performance, the nanocrystalline 7 wt.% In_2O_3-loaded SnO_2 thick-film sensors in this study have great potentials in practical application because the undesirable thermal growth could be limited due to the rather low operating temperature of 40–70 °C.

Interestingly, the 7 wt.% In_2O_3-loaded SnO_2 sensor was highly sensitive to low concentrations of H_2S gas even at room temperature. We hence speculated that in addition to the porous microstructure as well as the grain size effect, the n–N type heterojunction-based interfacial barriers between In_2O_3 and SnO_2 nanocrystals might be another mechanism accounting for the enhanced sensing performance. The heterogeneous band discontinuity between In_2O_3 and SnO_2 is shown in Fig. 9, with the electron affinity energy of In_2O_3 and SnO_2 taking values of about 3.5 eV [32] and 4.53 eV [33], respectively. Unlike homojunction, there is a spike on the In_2O_3 side along with a notch on SnO_2 side in the band diagram of interfaces. The band discontinuity sets barriers for electrons both in conduction band (~1.03 eV) and valence band (~1.23 eV), We believe that the In_2O_3–SnO_2 heterojunction interfacial barriers could strongly modify the charge transport behaviors of carriers since the carrier concentration varies exponentially with the barrier height. Further studies are required to determine the mechanism through which the In_2O_3–SnO_2 interfacial barriers promote the sensing performance toward gases like H_2S.

5. Conclusions

Nanocrystalline In_2O_3–SnO_2 thick films have been fabricated by standard screen-printing technique starting from hydrothermally synthesized SnO_2 and In_2O_3 nanopowders. The loading amount of indium oxide was varied from 0% to 9% by weight and it has been demonstrated that In_2O_3 loading has a distinct role in suppressing the crystallite growth and agglomeration of tetragonal rutile SnO_2 without appreciable structural modification when sintered at 700 °C. The optimal loading amount was found to be 7.0 wt.%, which offered the smallest crystallite size about 4.9 nm and highest sensor response toward H_2S gas in air with good selectivity. The 7 wt.% In_2O_3-loaded SnO_2 sensor had rather low optimal operating temperature (40 °C) as compared to pure SnO_2 (150 °C). Noteworthily, the 7 wt.% In_2O_3-loaded SnO_2 sensor was highly sensitive to low concentrations of H_2S even at room temperature, and exhibited fast and reproducible response when operated at 70 °C. The grain size effect, the interfacial barriers and porous microstructure might be responsible for the enhanced sensing performance.

Acknowledgements

This work was financially supported by National Natural Science Foundation of China (61006012) and Specialized Research Fund for the Doctoral Program of Higher Education of China (20070487182). The authors owe a lot to the Analytical and Testing Center at Huazhong University of Science and Technology for microstructure characterization.

References

[1] S.J. Pearton, F. Ren, Y.L. Wang, B.H. Chu, K.H. Chen, C.Y. Chang, W. Lim, J. Lin, D.P. Norton, Recent advances in wide bandgap semiconductor biological and gas sensors, Prog. Mater. Sci. 55 (2010) 1–59.

[2] G. Korotcenkov, S.D. Han, B.K. Cho, V. Brinzari, Grain size effects in sensor response of nanostructured SnO_2- and In_2O_3-based conductometric thin film gas sensor, Crit. Rev. Solid State Mater. Sci. 34 (2009) 1–17.

[3] Z.L. Wang, X.Y. Kong, Y. Ding, P.X. Gao, W.L. Hughes, R.S. Yang, Y. Zhang, Semiconducting and piezoelectric oxide nanostructures induced by polar surfaces, Adv. Funct. Mater. 14 (2004) 943–956.

[4] O.K. Tan, W. Cao, Y. Hu, W. Zhu, Nano-structured oxide semiconductor materials for gas-sensing applications, Ceram. Int. 30 (2004) 1127–1133.

[5] F. Pan, C. Song, X.J. Liu, Y.C. Yang, F. Zeng, Ferromagnetism and possible application in spintronics of transition-metal-doped ZnO films, Mater. Sci. Eng. R-Rep. 62 (2008) 1–35.

[6] N. Yamazoe, K. Shimanoe, New perspectives of gas sensor technology, Sens. Actuators B: Chem. 138 (2009) 100–107.

[7] S.P. Gong, H. Liu, D.X. Zhou, Progress in nanophase tin oxide gas sensors and gas-sensitive array, J. Inorg. Mater. 21 (2006) 521–526.

[8] G. Korotcenkov, Gas response control through structural and chemical modification of metal oxide films: state of the art and approaches, Sens. Actuators B: Chem. 107 (2005) 209–232.

[9] M.A. Ponce, M.S. Castro, C.M. Aldao, Resistance and capacitance analysis of Pd-doped and undoped SnO_2 thick films sensors exposed to CO atmospheres, Ceram. Int. 32 (2006) 733–737.

[10] T. Maekawa, J. Tamaki, N. Miura, N. Yamazoe, Sensing behavior of CuO-loaded SnO_2 element for H_2S detection, Chem. Lett. 4 (1991) 575–578.

[11] T. Maekawa, J. Tamaki, N. Miura, N. Yamzaoe, Improvement of copper oxide–tin oxide sensor for dilute hydrogen sulfide, J. Mater. Chem. 4 (1994) 1259–1262.

[12] L.A. Patil, D.R. Patil, Heterocontact type CuO-modified SnO_2 sensor for the detection of a ppm level H_2S gas at room temperature, Sens. Actuators B: Chem. 120 (2006) 316–323.

[13] S.P. Gong, J. Xia, J.Q. Liu, D.X. Zhou, Highly sensitive SnO_2 thin film with low operating temperature prepared by sol–gel technique, Sens. Actuators B: Chem. 134 (2008) 57–61.

[14] L. Francioso, A. Forleo, S. Capone, M. Epifani, A.M. Taurino, P. Siciliano, Nanostructured In_2O_3–SnO_2 sol–gel thin film as material for NO_2 detection, Sens. Actuators B: Chem. 114 (2006) 646–655.

[15] A. Forleo, L. Francioso, M. Epifani, S. Capone, A.M. Taurino, P. Siciliano, NO_2-gas-sensing properties of mixed In_2O_3–SnO_2 thin films, Thin Solid Films 490 (2005) 68–73.

[16] A.F. Chen, X.D. Huang, Z.F. Tong, S.L. Bai, R.X. Luo, C.C. Liu, Preparation, characterization and gas-sensing properties of SnO_2–In_2O_3 nanocomposite oxides, Sens. Actuators B: Chem. 115 (2006) 316–321.

[17] Z.A. Ansari, T.G. Ko, J.H. Oh, CO-sensing properties of In_2O_3-doped SnO_2 thick-film sensors: effect of doping concentration and grain size, IEEE Sens. J. 5 (2005) 817–824.

[18] G. Neri, A. Bonavita, G. Micali, G. Rizzo, N. Pinna, M. Niederberger, J. Ba, Effect of the chemical composition on the sensing properties of In_2O_3–SnO_2 nanoparticles synthesized by a non-aqueous method, Sens. Actuators B: Chem. 130 (2008) 222–230.

[19] H.M. Yang, X.C. Zhang, A.D. Tang, Mechanosynthesis and gas-sensing properties of In_2O_3/SnO_2 nanocomposites, Nanotechnology 17 (2006) 2860–2864.

[20] D.W. Chu, Y.P. Zeng, D.L. Jiang, Y. Masuda, In_2O_3–SnO_2 nano-toasts and nanorods: precipitation preparation, formation mechanism, and gas sensitive properties, Sens. Actuators B: Chem. 137 (2009) 630–636.

[21] S. Shukla, S. Seal, L. Ludwig, C. Parish, Nanocrystalline indium oxide-doped tin oxide thin film as low temperature hydrogen sensor, Sens. Actuators B: Chem. 97 (2004) 256–265.

[22] C. Drake, A. Amalu, J. Bernard, Enhancing the low temperature hydrogen sensitivity of nanocrystalline SnO_2 as a function of trivalent dopants, J. Appl. Phys. 101 (2007) 104307.

[23] A.F. Chen, S.L. Bai, B.J. Shi, Z.Y. Liu, D.Q. Li, C.C. Liu, Methane gas-sensing and catalytic oxidation activity of SnO_2–In_2O_3 nanocomposites incorporating TiO_2, Sens. Actuators B: Chem. 135 (2008) 7–12.

[24] T. Chen, Q.J. Liu, Z.L. Zhou, Y.D. Wang, A high sensitivity gas sensor for formaldehyde based on CdO and In_2O_3 doped nanocrystalline SnO_2, Nanotechnology 19 (2008) 095506.

[25] S.P. Gong, C. Xu, H. Liu, Hydrothermal synthesis of SnO_2 nanoparticles, Rare Metal Mat. Eng. 35 (2006) 583–585.

[26] W.J. Heward, D.J. Swenson, Phase equilibria in the pseudo-binary In_2O_3–SnO_2 system, J. Mater. Sci. 42 (2007) 7135–7140.

[27] H. Liu, S.P. Gong, Y.X. Hu, J.Q. Liu, D.X. Zhou, Properties and mechanism study of SnO_2 nanocrystals for H_2S thick-film sensors, Sens. Actuators B: Chem. 140 (2009) 190–195.

[28] N. Barsan, U. Weimar, Conduction model of metal oxide gas sensor, J. Electroceram. 7 (2001) 143–167.

[29] N. Yamazoe, G. Sakai, K. Shimanoe, Oxide semiconductor gas sensors, Catal. Surv. Asia 7 (2003) 63–75.

[30] C.N. Xu, J. Tamaki, N. Miura, N. Yamazoe, Grain size effect on gas sensitivity of porous SnO_2-based elements, Sens. Actuators B: Chem. 3 (1991) 147–155.

[31] S. Seal, S. Shukla, Nanocrystalline SnO gas sensors in view of surface reactions and modifications, JOM – J. Miner. Met. & Mater. Soc. 54 (2002) 35–38.

[32] Q.Y. Wang, K. Yu, F. Xu, J. Wu, Y. Xu, Z.Q. Zhu, Synthesis and field-emission properties of In_2O_3 nanostructures, Mater. Lett. 62 (2008) 2710–2713.

[33] M.N. Islam, M.O. Hakim, Electron affinity and work function of polycrystalline SnO_2 thin film, J. Mater. Sci. Lett. 5 (1986) 63–65.